



# Measurement of inclusive charmless semileptonic $B$ -meson decays at the endpoint of the electron momentum spectrum

Belle Collaboration

A. Limosani<sup>g</sup>, K. Abe<sup>g</sup>, K. Abe<sup>am</sup>, I. Adachi<sup>g</sup>, H. Aihara<sup>ao</sup>,  
Y. Asano<sup>as</sup>, T. Aushev<sup>k</sup>, S. Bahinipati<sup>d</sup>, A. M. Bakich<sup>aj</sup>,  
E. Barberio<sup>s</sup>, U. Bitenc<sup>l</sup>, I. Bizjak<sup>l</sup>, S. Blyth<sup>x</sup>, A. Bondar<sup>a</sup>,  
A. Bozek<sup>y</sup>, M. Bračko<sup>g,r,l</sup>, J. Brodzicka<sup>y</sup>, Y. Chao<sup>x</sup>, A. Chen<sup>v</sup>,  
K.-F. Chen<sup>x</sup>, W. T. Chen<sup>v</sup>, B. G. Cheon<sup>c</sup>, R. Chistov<sup>k</sup>,  
Y. Choi<sup>ai</sup>, A. Chuvikov<sup>af</sup>, S. Cole<sup>aj</sup>, J. Dalseno<sup>s</sup>, M. Danilov<sup>k</sup>,  
M. Dash<sup>at</sup>, J. Dragic<sup>g</sup>, A. Drutskoy<sup>d</sup>, S. Eidelman<sup>a</sup>,  
S. Fratina<sup>l</sup>, N. Gabyshev<sup>a</sup>, T. Gershon<sup>g</sup>, G. Gokhroo<sup>ak</sup>,  
B. Golob<sup>q,l</sup>, A. Gorišek<sup>l</sup>, T. Hara<sup>ac</sup>, N. C. Hastings<sup>ao</sup>,  
K. Hayasaka<sup>t</sup>, H. Hayashii<sup>u</sup>, M. Hazumi<sup>g</sup>, L. Hinz<sup>p</sup>,  
T. Hokuue<sup>t</sup>, Y. Hoshi<sup>am</sup>, S. Hou<sup>v</sup>, W.-S. Hou<sup>x</sup>, T. Iijima<sup>t</sup>,  
A. Imoto<sup>u</sup>, K. Inami<sup>t</sup>, A. Ishikawa<sup>g</sup>, R. Itoh<sup>g</sup>, M. Iwasaki<sup>ao</sup>,  
Y. Iwasaki<sup>g</sup>, J. H. Kang<sup>au</sup>, J. S. Kang<sup>n</sup>, N. Katayama<sup>g</sup>,  
H. Kawai<sup>b</sup>, T. Kawasaki<sup>aa</sup>, H. R. Khan<sup>ap</sup>, H. Kichimi<sup>g</sup>,  
H. J. Kim<sup>o</sup>, H. O. Kim<sup>ai</sup>, S. K. Kim<sup>ah</sup>, S. M. Kim<sup>ai</sup>,  
K. Kinoshita<sup>d</sup>, S. Korpar<sup>r,l</sup>, P. Krokovny<sup>a</sup>, R. Kulasiri<sup>d</sup>,  
S. Kumar<sup>ad</sup>, C. C. Kuo<sup>v</sup>, Y.-J. Kwon<sup>au</sup>, J. S. Lange<sup>e</sup>,  
G. Leder<sup>j</sup>, T. Lesiak<sup>y</sup>, J. Li<sup>ag</sup>, S.-W. Lin<sup>x</sup>, D. Liventsev<sup>k</sup>,  
J. MacNaughton<sup>j</sup>, G. Majumder<sup>ak</sup>, F. Mandl<sup>j</sup>,  
T. Matsumoto<sup>aq</sup>, Y. Mikami<sup>an</sup>, W. Mitaroff<sup>j</sup>, K. Miyabayashi<sup>u</sup>,  
H. Miyake<sup>ac</sup>, H. Miyata<sup>aa</sup>, R. Mizuk<sup>k</sup>, D. Mohapatra<sup>at</sup>,  
T. Mori<sup>ap</sup>, T. Nagamine<sup>an</sup>, Y. Nagasaka<sup>h</sup>, E. Nakano<sup>ab</sup>,  
M. Nakao<sup>g</sup>, Z. Natkaniec<sup>y</sup>, S. Nishida<sup>g</sup>, O. Nitoh<sup>ar</sup>,

T. Nozaki<sup>g</sup>, S. Ogawa<sup>al</sup>, T. Ohshima<sup>t</sup>, T. Okabe<sup>t</sup>, S. Okuno<sup>m</sup>,  
S. L. Olsen<sup>f</sup>, Y. Onuki<sup>aa</sup>, W. Ostrowicz<sup>y</sup>, H. Ozaki<sup>g</sup>,  
H. Palka<sup>y</sup>, C. W. Park<sup>ai</sup>, H. Park<sup>o</sup>, N. Parslow<sup>aj</sup>,  
R. Pestotnik<sup>l</sup>, L. E. Piilonen<sup>at</sup>, H. Sagawa<sup>g</sup>, Y. Sakai<sup>g</sup>,  
N. Sato<sup>t</sup>, T. Schietinger<sup>p</sup>, O. Schneider<sup>p</sup>, C. Schwanda<sup>j</sup>,  
R. Seuster<sup>f</sup>, M. E. Sevier<sup>s</sup>, H. Shibuya<sup>al</sup>, B. Shwartz<sup>a</sup>,  
V. Sidorov<sup>a</sup>, A. Somov<sup>d</sup>, R. Stamen<sup>g</sup>, S. Stanič<sup>as,1</sup>, M. Starič<sup>l</sup>,  
K. Sumisawa<sup>ac</sup>, T. Sumiyoshi<sup>aq</sup>, S. Y. Suzuki<sup>g</sup>, O. Tajima<sup>g</sup>,  
F. Takasaki<sup>g</sup>, K. Tamai<sup>g</sup>, N. Tamura<sup>aa</sup>, M. Tanaka<sup>g</sup>,  
Y. Teramoto<sup>ab</sup>, X. C. Tian<sup>ae</sup>, T. Tsukamoto<sup>g</sup>, S. Uehara<sup>g</sup>,  
K. Ueno<sup>x</sup>, T. Uglov<sup>k</sup>, S. Uno<sup>g</sup>, P. Urquijo<sup>s</sup>, G. Varner<sup>f</sup>,  
K. E. Varvell<sup>aj</sup>, S. Villa<sup>p</sup>, C. C. Wang<sup>x</sup>, C. H. Wang<sup>w</sup>,  
M.-Z. Wang<sup>x</sup>, Q. L. Xie<sup>i</sup>, B. D. Yabsley<sup>at</sup>, A. Yamaguchi<sup>an</sup>,  
H. Yamamoto<sup>an</sup>, Y. Yamashita<sup>z</sup>, M. Yamauchi<sup>g</sup>, J. Ying<sup>ae</sup>,  
J. Zhang<sup>g</sup>, L. M. Zhang<sup>ag</sup>, Z. P. Zhang<sup>ag</sup>, and D. Žontar<sup>q,l</sup>

<sup>a</sup>*Budker Institute of Nuclear Physics, Novosibirsk, Russia*

<sup>b</sup>*Chiba University, Chiba, Japan*

<sup>c</sup>*Chonnam National University, Kwangju, South Korea*

<sup>d</sup>*University of Cincinnati, Cincinnati, OH, USA*

<sup>e</sup>*University of Frankfurt, Frankfurt, Germany*

<sup>f</sup>*University of Hawaii, Honolulu, HI, USA*

<sup>g</sup>*High Energy Accelerator Research Organization (KEK), Tsukuba, Japan*

<sup>h</sup>*Hiroshima Institute of Technology, Hiroshima, Japan*

<sup>i</sup>*Institute of High Energy Physics, Chinese Academy of Sciences, Beijing, PR China*

<sup>j</sup>*Institute of High Energy Physics, Vienna, Austria*

<sup>k</sup>*Institute for Theoretical and Experimental Physics, Moscow, Russia*

<sup>l</sup>*J. Stefan Institute, Ljubljana, Slovenia*

<sup>m</sup>*Kanagawa University, Yokohama, Japan*

<sup>n</sup>*Korea University, Seoul, South Korea*

<sup>o</sup>*Kyungpook National University, Taegu, South Korea*

<sup>p</sup>*Swiss Federal Institute of Technology of Lausanne, EPFL, Lausanne, Switzerland*

<sup>q</sup>*University of Ljubljana, Ljubljana, Slovenia*

<sup>r</sup>*University of Maribor, Maribor, Slovenia*

<sup>s</sup>*University of Melbourne, Victoria, Australia*

<sup>t</sup>*Nagoya University, Nagoya, Japan*

- <sup>u</sup>*Nara Women's University, Nara, Japan*  
<sup>v</sup>*National Central University, Chung-li, Taiwan*  
<sup>w</sup>*National United University, Miao Li, Taiwan*  
<sup>x</sup>*Department of Physics, National Taiwan University, Taipei, Taiwan*  
<sup>y</sup>*H. Niewodniczanski Institute of Nuclear Physics, Krakow, Poland*  
<sup>z</sup>*Nihon Dental College, Niigata, Japan*  
<sup>aa</sup>*Niigata University, Niigata, Japan*  
<sup>ab</sup>*Osaka City University, Osaka, Japan*  
<sup>ac</sup>*Osaka University, Osaka, Japan*  
<sup>ad</sup>*Panjab University, Chandigarh, India*  
<sup>ae</sup>*Peking University, Beijing, PR China*  
<sup>af</sup>*Princeton University, Princeton, NJ, USA*  
<sup>ag</sup>*University of Science and Technology of China, Hefei, PR China*  
<sup>ah</sup>*Seoul National University, Seoul, South Korea*  
<sup>ai</sup>*Sungkyunkwan University, Suwon, South Korea*  
<sup>aj</sup>*University of Sydney, Sydney, NSW, Australia*  
<sup>ak</sup>*Tata Institute of Fundamental Research, Bombay, India*  
<sup>al</sup>*Toho University, Funabashi, Japan*  
<sup>am</sup>*Tohoku Gakuin University, Tagajo, Japan*  
<sup>an</sup>*Tohoku University, Sendai, Japan*  
<sup>ao</sup>*Department of Physics, University of Tokyo, Tokyo, Japan*  
<sup>ap</sup>*Tokyo Institute of Technology, Tokyo, Japan*  
<sup>aq</sup>*Tokyo Metropolitan University, Tokyo, Japan*  
<sup>ar</sup>*Tokyo University of Agriculture and Technology, Tokyo, Japan*  
<sup>as</sup>*University of Tsukuba, Tsukuba, Japan*  
<sup>at</sup>*Virginia Polytechnic Institute and State University, Blacksburg, VA, USA*  
<sup>au</sup>*Yonsei University, Seoul, South Korea*

---

## Abstract

We report measurements of partial branching fractions of inclusive charmless semileptonic  $B$ -meson decays at the endpoint of the electron momentum spectrum. The measurements are made in six overlapping momentum intervals that have lower bounds ranging from 1.9 GeV/ $c$  to 2.4 GeV/ $c$  and a common upper bound of 2.6 GeV/ $c$ , as measured in the centre of mass frame. The results are based on a sample of 29 million  $B\bar{B}$  pairs, accumulated by the Belle detector at the KEKB asymmetric  $e^+e^-$  collider operating on the  $\Upsilon(4S)$  resonance. In the momentum interval ranging from 1.9 GeV/ $c$  to 2.6 GeV/ $c$  we find  $|V_{ub}| = (4.49 \pm 0.42 \pm 0.32^{+0.21}_{-0.19}) \times 10^{-3}$ ,

where the first error is from experiment, the second is due to the uncertainty on HQET parameters and the third error is from theory.

*Key words:* Semileptonic  $B$ -meson decays; CKM matrix

*PACS:* 11.30.Er, 13.20.He, 12.15.Ff, 14.40.Nd

---

## 1 Introduction

The magnitude of the Cabibbo-Kobayashi-Maskawa (CKM) matrix element  $|V_{ub}|$  is a fundamental parameter of the Standard Model (SM). A knowledge of its value is crucial to the understanding of  $CP$  violation within the SM, which is underpinned by knowledge of the so-called Unitarity Triangle (UT). Recent precise measurements of UT angle  $\phi_1(\beta)$  [1,2] have focussed attention on  $|V_{ub}|$ , because it determines the side of the UT that is opposite  $\phi_1$ , it directly tests the Kobayashi-Maskawa mechanism [3] for  $CP$  violation within the SM.

To date, inclusive measurements of  $|V_{ub}|$  have been reported by experiments operating on the  $\Upsilon(4S)$  resonance, namely CLEO [4,5,6], ARGUS [7], BaBar [8] and Belle [9], and by LEP experiments operating on the  $Z$  resonance, namely L3 [10], ALEPH [11], DELPHI [12] and OPAL [13].

The value of  $|V_{ub}|$  can be extracted from the measured rate of charmless semileptonic  $B$ -meson decays  $B \rightarrow X_u e \nu_e$  in a kinematic region that has to be chosen to minimise the impact of the large background from the charmed semileptonic  $B$ -meson decays  $B \rightarrow X_c e \nu_e$ . One such region is at the endpoint of the lepton momentum spectrum: in the rest frame of the decaying  $B$  meson, leptons from  $B \rightarrow X_c e \nu_e$  decays attain a maximum momentum of 2.31 GeV/ $c$  whilst for  $B \rightarrow X_u e \nu_e$  decays the maximum is 2.64 GeV/ $c$ .

In this paper we report measurements of partial branching fractions to inclusive charmless semileptonic  $B$ -meson decays from the yield of electrons and positrons in six overlapping momentum intervals. The intervals have lower limits commencing at 1.9 GeV/ $c$  through to 2.4 GeV/ $c$  incremented in steps of 0.1 GeV/ $c$  and a common upper limit of 2.6 GeV/ $c$ , as measured in the centre of mass (CM)<sup>2</sup> frame.

We use two methods to extract  $|V_{ub}|$ , one that has been standard practice [19] (DFN), and one that has been recently developed [14,15,16,17,18](BLNP). The DFN method involves extrapolation from a partial to a full branching

---

<sup>1</sup> on leave from Nova Gorica Polytechnic, Nova Gorica, Slovenia

<sup>2</sup> The  $\Upsilon(4S)$  frame is equivalent to the centre of mass frame.

fraction using the DeFazio-Neubert prescription with given shape function parameters [20] followed by a routine to translate full branching fraction to  $|V_{ub}|$  [19]. We determine the shape function parameters using the  $B \rightarrow X_s \gamma$  photon energy spectrum as measured by Belle [21,22]<sup>3</sup>. In contrast to the DFN method the BLNP method provides a more systematic treatment of shape function effects by incorporating all known contributions, includes power corrections, uses an improved perturbative treatment and directly relates the partial rates of  $B \rightarrow X_u e \nu_e$  to  $|V_{ub}|$ . In this implementation of the method the shape function parameters are constrained by measurements of HQET parameters from semileptonic and radiative  $B$ -meson decays [18,25].

## 2 Detector and Data Sample

The results reported here are based on data collected with the Belle detector at the KEKB asymmetric energy  $e^+e^-$  collider [26]. The Belle detector is a large-solid-angle magnetic spectrometer that consists of a three-layer silicon vertex detector (SVD), a 50-layer central drift chamber (CDC), an array of aerogel threshold Čerenkov counters (ACC), a barrel-like arrangement of time-of-flight scintillation counters (TOF), and an electromagnetic calorimeter comprised of CsI(Tl) crystals (ECL) located inside a superconducting solenoid coil that provides a 1.5 T magnetic field. An iron flux-return located outside of the coil is instrumented to detect  $K_L^0$  mesons and to identify muons (KLM). The detector is described in detail elsewhere [27]. We use 27.0 fb<sup>-1</sup> and 8.8 fb<sup>-1</sup> integrated luminosity samples taken at (ON) and 60 MeV below (OFF) the  $\Upsilon(4S)$  resonance energy, respectively. The ON sample consists of 29.4 million  $B\bar{B}$  events. Unless explicitly stated otherwise, all variables are calculated in the CM frame.

## 3 Data Analysis

The procedure for this analysis largely follows that of CLEO [6], and consists of examining the spectrum of electron candidates with momentum in the range 1.5 – 3.5 GeV/ $c$ , which includes both signal and sideband regions. Our main background suppression selection criteria are optimised for the momentum region, 2.2 – 2.6 GeV/ $c$ , and based on the result of the CLEO analysis at the endpoint [6]. For ease of explanation we discuss the experimental procedure

---

<sup>3</sup> The use of the photon energy spectrum from inclusive radiative  $B$ -meson decays in determining the  $b$ -quark shape function or distribution function was first discussed by Bigi *et al* [23] and Neubert [24].

with respect to this momentum interval and later describe the slight differences encountered in the signal extraction for other momentum intervals.

In the CM frame the kinematic endpoint of decays of the type  $B \rightarrow X_c e \nu_e$ , including the non-zero  $B$  momentum and detector effects, is 2.4 GeV/ $c$ . The  $B \rightarrow X_u e \nu_e$  signal is extracted in the momentum region 2.2 – 2.6 GeV/ $c$  (HI), while a lower range, from 1.5 – 2.2 GeV/ $c$  (LO), is examined to evaluate the contribution from  $B \rightarrow X_c e \nu$ , which is then extrapolated to the HI region.

The uncertainty on the fraction of  $B \rightarrow X_u e \nu$  within the HI region is a major source of systematic error for the determination of the branching fraction and  $|V_{ub}|$ . For choosing and optimising selection criteria we use a sample of events containing  $B \rightarrow X_u e \nu_e$  decays, generated via Monte Carlo simulation and based on a model described in Ref. [28] (ISGW2). We also generate samples based on an inclusive  $B \rightarrow X_u e \nu_e$  model, according to the prescription of DeFazio and Neubert [20], with shape function (SF) parameters that correspond to the the residual  $B$ -meson mass<sup>4</sup> and the average momentum squared of the  $b$ -quark inside the  $B$ -meson set to  $\Lambda^{\text{SF}} = 0.659 \text{ GeV}/c^2$  and  $-\lambda_1^{\text{SF}} = 0.400 \text{ GeV}^2/c^2$ , respectively. These values were determined from the photon energy spectrum in  $B \rightarrow X_s \gamma$  decays measured by Belle [22]. To examine the extent to which our results may vary due to uncertainties in  $\Lambda^{\text{SF}}$  and  $\lambda^{\text{SF}}$ , we also generate four samples with parameters that define the long and short axes of the  $1\sigma$  contour in the  $(\frac{\Lambda^{\text{SF}}}{\text{GeV}/c^2}, \frac{\lambda_1^{\text{SF}}}{\text{GeV}^2/c^2})$  plane, corresponding to (0.614, -0.231), (0.736, -0.714), (0.719, -0.462) and (0.635, -0.483).

### 3.1 Event Selection

To select hadronic events we require the multiplicity of tracks to be greater than four and the primary event vertex to be within 1.5 cm radial and 3.5 cm longitudinal separation from the detector origin. We make further requirements based on quantities calculated in the CM frame – that the sum of cluster energies in the ECL satisfies  $0.18\sqrt{s} < E_{\text{ECL}} < 0.80\sqrt{s}$  where  $\sqrt{s}$  is the collision energy, that the visible energy  $E_{\text{vis}}$  be at least  $0.50\sqrt{s}$ , that the absolute sum of longitudinal track and photon momenta be less than  $0.30\sqrt{s}$ , that the heavy jet mass be either at least  $0.25 \times E_{\text{vis}}$  or greater than 1.8 GeV/ $c^2$ , and that the average cluster energy be less than 1 GeV. We also require that the ratio  $R_2$  of the second to the zeroth Fox-Wolfram moment [29] be less than 0.5.

---

<sup>4</sup>  $\Lambda^{\text{SF}} = M_B - m_b$ ;

where  $m_b$  and  $M_B$  are the masses of the  $b$ -quark and  $B$ -meson, respectively.

### 3.2 Electron spectrum

Charged tracks are reconstructed from hits in the SVD and the CDC. Tracks are required to pass within a short distance from the interaction point (IP) of the  $e^+e^-$  collision, where the  $B$ -meson decays promptly. For improved data and MC agreement, tracks must be within the acceptance of the barrel part of the ECL;  $-0.63 < \cos \theta_{\text{lab}} < 0.85$ , where  $\theta_{\text{lab}}$  is the polar angle measured in the laboratory frame with respect to the direction opposite to that of the positron beam. Tracks are identified as electrons on the basis of a matching energy cluster in the ECL, and, subsequently, upon the ratio of ECL-measured energy to CDC-measured track momentum, transverse shower shape in the ECL, ionisation energy loss in the CDC, and the ACC light yield [30]. Given the track requirements, electrons with momenta in the range  $1.5 - 2.6 \text{ GeV}/c$  are positively identified with a probability of  $(94.0 \pm 1.5)\%$  whilst pions are misidentified as electrons with a probability of  $(0.13 \pm 0.01)\%$ , as measured using samples of reconstructed  $J/\psi \rightarrow e^+e^-$  and  $K_S^0 \rightarrow \pi^+\pi^-$  decays, respectively.

To reduce the contribution of electrons from  $J/\psi$  and  $\psi(2S)$  decays and photon conversions, our candidate electrons are paired with oppositely charged tracks identified as electrons in the event and rejected if their mass falls within either  $J/\psi$ ,  $\psi(2S)$  or  $\gamma$  mass windows, defined as  $[3.025, 3.125] \text{ GeV}/c^2$ ,  $[3.614, 3.714] \text{ GeV}/c^2$  and  $[0, 0.1] \text{ GeV}/c^2$ , respectively. The photon conversion veto has the additional effect of removing electrons from  $\pi^0$  Dalitz decays. The yields of candidates that do not pass the  $J/\psi$  veto requirement are compared in data and MC to determine a normalisation factor for MC-estimated backgrounds, which are described below.

Since the dynamics of the hadronic part of  $B \rightarrow X_u e \nu_e$  is not well established, it is important that selection requirements retain acceptance over a wide range of  $q^2 \equiv (p_e + p_\nu)^2$  (dilepton invariant mass squared) in order to minimise model dependence. Additional event requirements are designed to reduce contributions from continuum ( $e^+e^- \rightarrow q\bar{q}$  where  $q = u, d, s, c$ ) and QED-related processes (including two photon and tau-pair events) without introducing a  $q^2$  bias. A set of “energy flow” variables is formed by grouping detected particles in bins of 0.05 in  $\cos \theta$ , where  $\theta$  is the particle angle with respect to the candidate electron, and taking the energy sum in each bin. The energy flow in the backward direction  $-1.00 < \cos \theta < -0.95$  is not used, as it is found to disproportionately reduce the acceptance in the low  $q^2$  region. A Fisher discriminant, denoted  $\mathcal{F}_{\text{FLOW}}$ , is constructed from the remaining energy flow variables with coefficients chosen to best separate signal from continuum events. We also make use of a  $b$ -quark rare decay tag variable, denoted  $\mathcal{K}$ , and

calculated as

$$\mathcal{K} = Q(e) \left( N(K^+) - N(K^-) \right), \quad (1)$$

where  $Q(e)$  is the charge of the candidate electron, and  $N(K^\pm)$  are the number of tracks identified as positively and negatively charged kaons in an event, respectively.  $\mathcal{K}$  exploits the presence of lepton-kaon charge correlations evident in  $B\bar{B}$  events wherein one  $B$ -meson decays via a  $b \rightarrow ue\nu_e$  transition whilst the other  $B$ -meson decays typically via  $\bar{b} \rightarrow \bar{c} \rightarrow \bar{s}$  transitions, thereby resulting in, on average, a net strangeness or kaon charge that is correlated to the charge of our candidate electron. The correlation does not exist in continuum events nor in  $B\bar{B}$  events that do not involve the  $b \rightarrow ue\nu_e$  transition. Charged tracks are identified as kaons by utilising specific ionisation energy loss measurements made with the CDC, light yield readings from the ACC, and time of flight information from the TOF. The average kaon identification efficiency and fake rate in the momentum range 0.5–4.0 GeV/ $c$ , as measured in the laboratory frame, are  $(88.0 \pm 0.1)\%$  and  $(8.5 \pm 0.1)\%$ , respectively.

To preserve signal efficiency, the selection requirements on  $\mathcal{F}_{\text{FLOW}}$  are chosen differently for three cases of  $\mathcal{K}$ :  $\mathcal{K} > 0$ ;  $\mathcal{K} = 0$ ; and  $\mathcal{K} < 0$ . The cut values are chosen to optimise the figure of merit  $S/\sqrt{S+B}$ , where  $S$  and  $B$  reflect the signal and continuum background expectation, respectively, as estimated from MC events, assuming the branching fraction measured by CLEO [6]. The  $\mathcal{K}$  dependent cuts on  $\mathcal{F}_{\text{FLOW}}$  reduce continuum backgrounds by 97% while retaining 33% of the  $B \rightarrow X_u e \nu_e$  signal.

To further suppress QED-related continuum backgrounds, the cosine of the angle between the thrust axis of the event and the  $e^-$  direction  $\cos \theta_{thr}$ , is required to be less than 0.75. Crucially, the thrust axis calculation includes the missing momentum as a component. Missing momentum is calculated as the difference between the momentum of the beams and the sum of the observed track and cluster momenta. Placing a constraint on  $\cos \theta_{thr}$  was found to bias the  $q^2$  distribution in signal events less than a constraint imposed on the direction of missing momentum, which has been previously used by CLEO [6]. The requirement on  $\cos \theta_{thr}$  reduces QED-related continuum backgrounds by 50% with a signal inefficiency of 10%.

The acceptance of the selection requirements as a function of generated  $q^2$  for events containing electrons in the momentum interval 2.2 – 2.6 GeV/ $c$  from  $B \rightarrow X_u e \nu_e$  decay is shown in Figure 1.

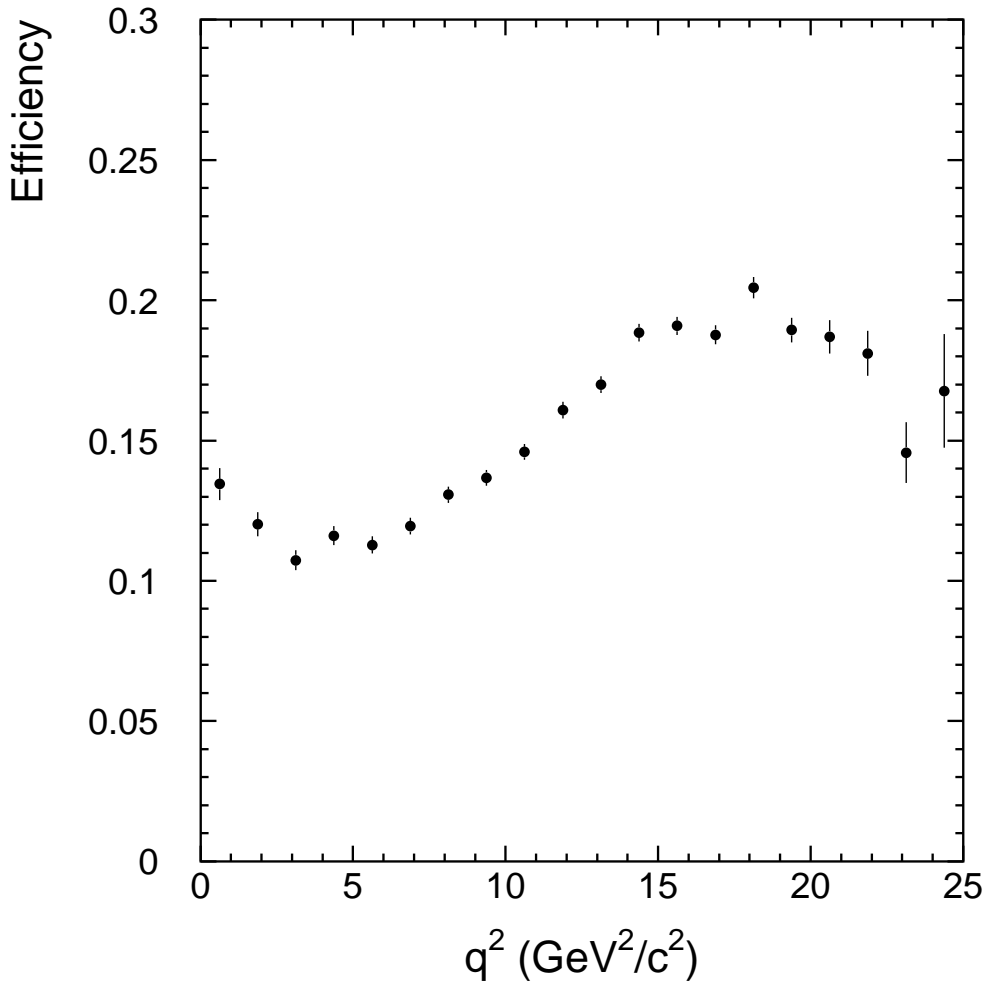


Fig. 1. Acceptance of the selection requirements as a function of generated  $q^2$  for events containing electrons in the region 2.2-2.6 GeV/ $c$  from  $B \rightarrow X_u e \nu_e$  decay.

### 3.3 Backgrounds

Sources of background for  $B \rightarrow X_u e \nu_e$  include continuum events, hadrons misidentified as electrons (“fakes”), charm bearing decays  $B \rightarrow X_c e \nu_e$ , and various secondary decays of  $B$ -mesons. We describe below our evaluation of each as well as our procedures for evaluating the associated contributions to the systematic uncertainty.

The continuum contribution is evaluated using the OFF data set. To account for the small difference in the momentum spectra due to the beam energy difference (0.6%), the electron momenta in OFF data are scaled by the ratio of ON to OFF CM energies. The yields in OFF data are then scaled by the factor  $\alpha = 3.005 \pm 0.015$ , determined by the ON to OFF ratio of Bhabha event

yields in the barrel ECL. As a check of this procedure, we measure the yields in the momentum range  $2.8 - 3.5$  GeV/ $c$ , above the kinematic maximum for  $B\bar{B}$  events. The resulting signal of  $85 \pm 93$  electron candidates is consistent with zero, as expected. We assign systematic uncertainties based on a MC study of the detector response to Bhabha events (0.4%), and the discrepancy with  $\alpha$  as calculated, similarly, with dimuon events (0.2%).

The remaining contributions to background are from  $B\bar{B}$  events and are estimated using a large Monte Carlo simulated sample of generic  $B\bar{B}$  events [31] that contains roughly three and a half times the number of  $B\bar{B}$  events in the ON sample. The MC yield due to fakes from charged pions is corrected for the difference in fake efficiency measured by data and MC samples of  $K_S^0 \rightarrow \pi^+\pi^-$  decays. The error on the correction ( $\sim 30\%$ ) is assigned as the systematic uncertainty on the yield from pions. Additional minor contributions from kaons, protons and muons to the overall fakes yield are conservatively assigned systematic uncertainties of 100%.

Of the real electrons, those not from primary  $B \rightarrow X_c e \nu_e$ , secondary backgrounds, are estimated using the Monte Carlo simulated generic  $B\bar{B}$  event sample with electronic branching fractions of  $D^0$ ,  $D^+$ ,  $J/\psi$ ,  $\psi(2S)$ ,  $D_s$  and  $\tau$  assigned according to the current world averages [32]. To avoid any bias from a possible mis-modelling of data in MC we use the vetoed  $J/\psi$  sample to measure the normalisation factor for both fake and secondary background MC yields. This factor is calculated from a fit of the MC-simulated momentum spectrum of vetoed electron candidates from  $J/\psi$  in  $B$ -meson decays to the equivalent spectrum obtained from the data. This sample is statistically independent of the final event sample, and, moreover, may not contain neutrinos from primary  $B$ -meson decays, which is the case for events providing fake and secondary backgrounds. Contributions from secondary electrons are assigned systematic errors based on the electronic branching fraction uncertainties and the difference between the MC normalisation calculated as described above and that according to the number of  $\Upsilon(4S)$  events (6%). Overall, the latter uncertainty has a less than 0.5% effect on the eventual signal yield.

The spectrum from  $B \rightarrow X_c e \nu_e$  is modelled using three components:  $X_c = D$  (HQET [33]);  $D^*$  (HQET [33]); and higher resonance charm meson states  $D^{**}$  (ISGW2). To improve the correspondence with observation, we re-weight the  $D$  and  $D^*$  components according to  $q^2$  in order to match spectra generated with world average values of form factors [32]. The ratio of  $D$  to  $D^*$  branching fractions is fixed according to their world average measurements [32]. The proportion of the  $(D + D^*)$  component with respect to the  $D^{**}$  component is determined from a binned maximum likelihood fit [34] of the ON data in the LO region <sup>5</sup>, where the  $B \rightarrow X_u e \nu_e$  component

---

<sup>5</sup> The sum of the yields of the components in the fit is constrained to equal the ON

is modelled using the inclusive model described earlier and fixed such that  $\mathcal{B}(B \rightarrow X_u e \nu_e) = (0.25 \pm 0.20)\%$  [19]. For the  $D^{**}$  sub-components,  $D_1$  and  $D_2^*$  we set  $\frac{\mathcal{B}(B \rightarrow D_1 e \nu_e) + \mathcal{B}(B \rightarrow D_2^* e \nu_e)}{\mathcal{B}(B \rightarrow D^{**} e \nu_e)} = 0.35 \pm 0.23$ , which has been determined by averaging maximum and minimum assessments of their respective world average branching fractions [32]. Semileptonic spectra are also re-weighted to include the effect of QED radiative corrections as calculated with the PHOTOS algorithm [35]. It has been observed that the KEKB collision energy has variations of  $\sim 1$  MeV over time and that this results in a measurable variation of the  $B$ -meson momentum over the running period of our ON data sample. As our Monte Carlo generator assumes a fixed energy, we apply a shift to the reconstructed momentum in the MC to correct for the difference. The correction depends on the beam energy measurement in the same run period as our ON data set, which is made using a fully reconstructed  $B$ -meson decay sample. All spectra for backgrounds other than  $B \rightarrow X_c e \nu_e$  are derived from the generic  $B\bar{B}$  MC sample and handled in the same manner as for the HI region. The goodness-of-fit as estimated by the  $\chi^2/\text{ndf}$  gives 17.8/13. We use this fit result to not only determine the  $B \rightarrow X_c e \nu_e$  background level in the HI region ( $2.2 - 2.6$  GeV/ $c$ ), but also simultaneously in the signal regions defined as  $2.3 - 2.6$  GeV/ $c$  and  $2.4 - 2.6$  GeV/ $c$ .

The same procedure as described above is repeated for three additional HI regions  $1.9 - 2.6$  GeV/ $c$ ,  $2.0 - 2.6$  GeV/ $c$ , and  $2.1 - 2.6$  GeV/ $c$ . In each case the LO region is adjusted such that its upper bound equals the lower bound of the HI region, giving respective LO regions of:  $1.5 - 1.9$  GeV/ $c$ ;  $1.5 - 2.0$  GeV/ $c$ ; and  $1.5 - 2.1$  GeV/ $c$ . The  $\chi^2/\text{ndf}$  for fits in these LO regions are: 6.8/7; 11.9/9; and 13.9/11, respectively.

The systematic error on our measurement due to the uncertainty in the  $B \rightarrow X_c e \nu_e$  shape and relative normalisations is estimated by varying the parameters fixed in the fit by their individual uncertainties, as described above. The maximum deviation observed from either an upward or downward variation is assigned as the systematic error. We also calculate uncertainties for each case of no QED radiative correction, an ISGW2 modelled  $B \rightarrow X_u e \nu_e$  spectrum shape, and the inclusion of a non-resonant  $B \rightarrow D^{(*)} \pi e \nu_e$  (Goity and Roberts [36]) decay component in the fit. CLEO included this component in their standard fit [6], but in our case, the shape of its momentum spectrum bears too close a resemblance to that of the  $B \rightarrow D^{**} e \nu_e$  component, which when included in the fit, results in either a non-zero  $D^{(*)} \pi$  and a zero  $D^{**}$  component or vice versa. The former is clearly contrary to observation, given the measured inclusive branching fraction  $\mathcal{B}(B \rightarrow D^{**} e \nu) = (2.70 \pm 0.70)\%$  [32].

The systematic that has the greatest effect on the  $X_c$  background estimation in the HI region is the uncertainty on the  $D^*$  form factor, which has been

---

data yield.

obtained by varying the form factor slope parameter  $\rho^2$  within its uncertainty. The net systematic uncertainty is calculated as a sum in quadrature. Table 1 lists the electron candidate yields in ON data, the estimated background contributions and the subsequent extracted signal for the six overlapping momentum intervals.

Table 1

The  $B \rightarrow X_u e \nu_e$  endpoint and background yields in six momentum intervals, where the first error is statistical and the second is systematic.

$p_{\text{CM}} \text{ (GeV}/c\text{)}$	2.4 – 2.6	2.3 – 2.6	2.2 – 2.6
$N_{\text{ON}}$	1741	3534	8854
$\alpha N_{\text{OFF}}$	$1166 \pm 59 \pm 5$	$1878 \pm 75 \pm 8$	$2743 \pm 91 \pm 11$
Fakes	$12 \pm 2 \pm 4$	$43 \pm 4 \pm 14$	$85 \pm 5 \pm 28$
$N_{B \rightarrow J/\psi \rightarrow e}$	$40 \pm 3 \pm 4$	$94 \pm 5 \pm 8$	$191 \pm 7 \pm 17$
$N_{B \rightarrow X \rightarrow e}$	$8 \pm 1 \pm 1$	$23 \pm 2 \pm 2$	$53 \pm 4 \pm 4$
$N_{B \rightarrow X_c e \nu_e}$	$4 \pm 1 \pm 0$	$345 \pm 11 \pm 23$	$3658 \pm 36 \pm 151$
$N_{B \rightarrow X_u e \nu_e}$	$512 \pm 73 \pm 7$	$1152 \pm 97 \pm 29$	$2124 \pm 136 \pm 155$

$p_{\text{CM}} \text{ (GeV}/c\text{)}$	2.1 – 2.6	2.0 – 2.6	1.9 – 2.6
$N_{\text{ON}}$	23617	54566	104472
$\alpha N_{\text{OFF}}$	$3738 \pm 106 \pm 15$	$4900 \pm 121 \pm 20$	$6234 \pm 137 \pm 25$
Fakes	$93 \pm 6 \pm 34$	$131 \pm 7 \pm 40$	$143 \pm 9 \pm 47$
$N_{B \rightarrow J/\psi \rightarrow e}$	$336 \pm 9 \pm 29$	$562 \pm 12 \pm 49$	$880 \pm 15 \pm 77$
$N_{B \rightarrow X \rightarrow e}$	$127 \pm 5 \pm 10$	$263 \pm 8 \pm 22$	$553 \pm 11 \pm 48$
$N_{B \rightarrow X_c e \nu_e}$	$15494 \pm 73 \pm 437$	$42769 \pm 123 \pm 970$	$87705 \pm 180 \pm 1550$
$N_{B \rightarrow X_u e \nu_e}$	$3830 \pm 201 \pm 439$	$5941 \pm 291 \pm 972$	$8957 \pm 395 \pm 1553$

#### 4 Extraction of partial branching fraction

The inclusive partial branching fraction is found using

$$\Delta\mathcal{B} = \frac{N(B \rightarrow X_u e \nu)}{2N_{B\bar{B}}\epsilon_{\text{MC}}} \quad (2)$$

where  $N_{B\bar{B}} = (29.4 \pm 0.4) \times 10^6$  and the overall selection efficiency is  $\epsilon_{\text{MC}}$ . The systematic uncertainty on the efficiency includes effects from tracking, electron identification, event selection, or model criteria:

- The uncertainty on the track finding for our electron candidates is studied using the MC simulated track embedding method. Care is taken to consider all known sources of uncertainty in the MC simulation: magnetic field effects; CDC wire hit inefficiency; uncertainties in the material budget of the SVD and CDC; and drift time resolution effects in the CDC. The ratio of data to MC single track reconstruction efficiency is consistent with unity at the level of a 1%. Accordingly, this uncertainty is assigned as the systematic error on the efficiency due to tracking;
- The uncertainty in electron identification (ID) efficiency is measured using inclusive  $J/\psi$  events (The method implemented is similar to that described in Ref. [30]). The study involves reconstructing  $J/\psi \rightarrow e^+e^-$  decays with both tracks satisfying the same track requirements as those met by electron candidates considered for this analysis. We find excellent agreement of the MC simulation with data at the level of 2% and subsequently assign this as the systematic uncertainty on electron identification;
- The effect of the main event selection criteria, namely those of  $\mathcal{K}$  dependent  $\mathcal{F}_{\text{FLOW}}$  and  $\cos\theta_{thr}$  cuts, is assessed in two control samples. We fully reconstruct  $B^+ \rightarrow \bar{D}^0(\rightarrow K^+\pi^-)\rho^+(\rightarrow \pi^+\pi^0)$  decays. Here the kaon, disregarding particle identification, is assigned as the electron candidate, whilst the pion is regarded as the neutrino. In comparison to  $B \rightarrow X_u e \nu_e$ , the mass of the  $D$  meson fixes the study to  $q^2 = m_D^2$ . The data to MC ratio of the selection efficiency is calculated as a function of CM momentum in the range  $1.5 - 2.6$  GeV/ $c$ , in bins of 0.05 GeV/ $c$ ; the best fit is achieved with a constant, which is found to be consistent with unity within 2% uncertainty. We also fully reconstruct  $J/\psi \rightarrow e^+e^-$  decays and subtract off backgrounds to yield  $B \rightarrow J/\psi X$  decays. We assign the highest momentum electron from the  $J/\psi$  decay to be the electron candidate. The remaining electron is regarded as the neutrino. The mass of the  $J/\psi$ -meson fixes the study to  $q^2 = m_{J/\psi}^2$ . The selection efficiency in this sample was measured as described above, and the best fit, which was also achieved with a constant, found data and MC agree to within 3% uncertainty. Accordingly an overall uncertainty of 4% is assigned as the systematic error due to event selection;
- Model dependence is assessed using the four inclusive samples described above. The maximum shift in selection efficiency is assigned as the systematic uncertainty due to model dependence, and is dependent upon the particular HI region. It varies from 1.7% to 3.4% as the lower momentum limit is increased.

The efficiencies for selecting electrons from  $B \rightarrow X_u e \nu_e$  decays after all selection criteria have been applied are given in Table 2. Our total efficiency decreases as the the lower limit of the electron momentum interval increases,

Table 2

Branching fractions and extraction of  $|V_{ub}|$  (standard method). The reconstruction efficiency,  $\epsilon_{\text{MC}}$ , as calculated from Monte Carlo. The partial branching fractions,  $\Delta\mathcal{B}_u(p)$ , where the errors are from statistics and experimental systematics, respectively. The lepton momentum spectral fractions,  $f_u$ , where the first error is the combined statistical and systematic uncertainty, and the second error is the theoretical uncertainty in extracting shape function parameters from  $B \rightarrow X_s \gamma$  decays and applying this knowledge to  $B \rightarrow X_u l \nu_l$  decays. The corrections due to the final state radiation loss  $\delta_{\text{RAD}}$ . The full branching fractions,  $\mathcal{B}(B \rightarrow X_u l \nu_l)$ , where the first error is due to experimental uncertainty and the second is from  $f_u$ . The extracted values of  $|V_{ub}|$ : the first error is experimental; the second error is from  $f_u$ , combined statistical and systematic; the third error is from  $f_u$  theory; and the last is from the application of the  $|V_{ub}|$  formula given in Eqn 3.

$p_{\text{CM}} (\text{GeV}/c)$	$\epsilon_{\text{MC}} (\%)$	$\Delta\mathcal{B}_u(p) (10^{-4})$	$f_u$
1.9 – 2.6	$18.0 \pm 0.9$	$8.47 \pm 0.37 \pm 1.53$	$0.321 \pm 0.022 \pm 0.041$
2.0 – 2.6	$17.6 \pm 0.9$	$5.74 \pm 0.28 \pm 0.98$	$0.246 \pm 0.020 \pm 0.042$
2.1 – 2.6	$17.2 \pm 0.9$	$3.78 \pm 0.20 \pm 0.48$	$0.173 \pm 0.017 \pm 0.040$
2.2 – 2.6	$16.6 \pm 0.9$	$2.17 \pm 0.14 \pm 0.20$	$0.109 \pm 0.013 \pm 0.034$
2.3 – 2.6	$16.5 \pm 0.9$	$1.18 \pm 0.10 \pm 0.07$	$0.058 \pm 0.010 \pm 0.025$
2.4 – 2.6	$16.2 \pm 1.0$	$0.53 \pm 0.07 \pm 0.03$	$0.025 \pm 0.006 \pm 0.014$
$p_{\text{CM}} (\text{GeV}/c)$	$\delta_{\text{RAD}}$	$\mathcal{B}(B \rightarrow X_u e \nu_e) (10^{-3})$	$ V_{ub}  (10^{-3})$
1.9 – 2.6	$0.06 \pm 0.02$	$2.80 \pm 0.52 \pm 0.41$	$5.01 \pm 0.47 \pm 0.17 \pm 0.32 \pm 0.24$
2.0 – 2.6	$0.07 \pm 0.02$	$2.49 \pm 0.45 \pm 0.47$	$4.73 \pm 0.42 \pm 0.19 \pm 0.40 \pm 0.23$
2.1 – 2.6	$0.07 \pm 0.02$	$2.34 \pm 0.33 \pm 0.59$	$4.59 \pm 0.32 \pm 0.22 \pm 0.53 \pm 0.22$
2.2 – 2.6	$0.09 \pm 0.03$	$2.16 \pm 0.25 \pm 0.73$	$4.41 \pm 0.25 \pm 0.27 \pm 0.69 \pm 0.21$
2.3 – 2.6	$0.10 \pm 0.03$	$2.22 \pm 0.24 \pm 1.02$	$4.47 \pm 0.24 \pm 0.36 \pm 0.96 \pm 0.22$
2.4 – 2.6	$0.11 \pm 0.04$	$2.39 \pm 0.38 \pm 1.46$	$4.63 \pm 0.37 \pm 0.53 \pm 1.32 \pm 0.22$

an effect due mostly to the momentum dependence of the  $\mathcal{K}$  dependent  $\mathcal{F}_{\text{FLOW}}$  cut.

Figure 2(a) shows the ON and scaled OFF momentum spectra along with the total background. Figure 2(b) shows the ON spectrum after background subtraction and efficiency correction, revealing the contribution of  $B \rightarrow X_u e \nu_e$ . The shape prescribed by the inclusive model described earlier, with final state radiation, is also shown. The partial branching fractions for each momentum interval are given in Table 2; as the lower momentum limit is decreased the uncertainty comes to be dominated, as expected, by the uncertainty in the  $B \rightarrow X_c e \nu_e$  background subtraction.

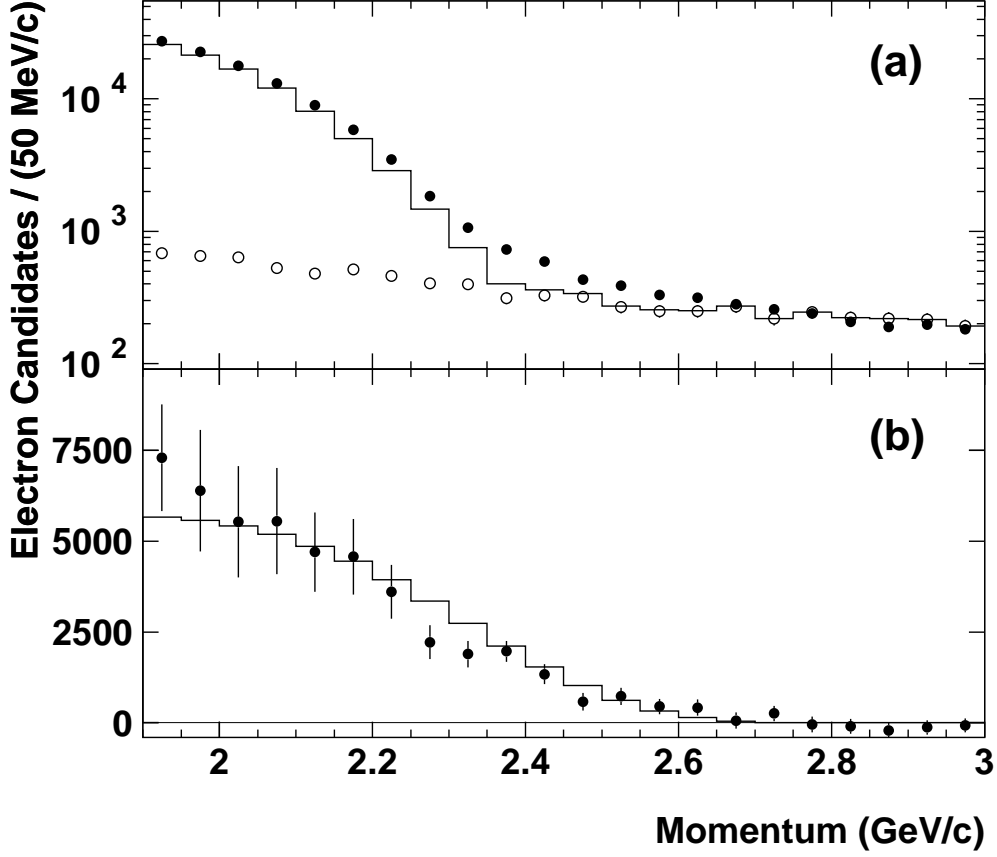


Fig. 2. The electron momentum spectrum in the  $\Upsilon(4S)$  rest frame: (a) ON data (filled circles), scaled OFF data (open circles), sum of scaled OFF data and estimated  $B\bar{B}$  backgrounds (histogram). (b) ON data after subtraction of backgrounds and correction for efficiency (filled circles) and model spectrum of  $B \rightarrow X_u e \nu_e$  decays with final state radiation (histogram, normalised to the data yield in the 1.9 – 2.6 GeV/c momentum range).

## 5 Extraction of $|V_{ub}|$

### 5.1 DFN method

The value of  $|V_{ub}|$  is extracted using the formula given in Ref. [19]:

$$|V_{ub}| = 0.00424 \sqrt{\frac{\mathcal{B}(B \rightarrow X_u e \nu_e)}{0.002} \frac{1.604 \text{ ps}}{\tau_B}} \times (1.0 \pm 0.028_{\lambda_{1,2}} \pm 0.039_{m_b}), \quad (3)$$

which is an updated version of the expression given in Ref. [32], and includes the latest measurements of the heavy-quark expansion parameters [37]. We average the current world average neutral and charged  $B$ -meson lifetimes to obtain  $\tau_B = 1.604 \pm 0.011$  ps [32]. To obtain the full inclusive rates for charmless semileptonic  $B$ -meson decay from our partial branching fractions, we must determine the spectral fractions  $f_u$  and the spectral distortion due to final state radiation loss  $\delta_{\text{RAD}}$  such that

$$\mathcal{B}(B \rightarrow X_u e \nu_e) = \frac{\Delta \mathcal{B}(B \rightarrow X_u e \nu_e)}{f_u} (1 + \delta_{\text{RAD}}). \quad (4)$$

The value of  $\delta_{\text{RAD}}$  is calculated from a comparison of MC signal events with and without the PHOTOS algorithm implemented. It has been the convention to assign a 10% systematic uncertainty on the correction based on studies that compare the PHOTOS performance with next-to-leading order calculations in  $B \rightarrow D e \nu_e$  decays [38], since the study has yet to be extended to  $B \rightarrow X_u e \nu_e$  decays, we assign a larger uncertainty, equivalent to a third of the size of the effect. The correction factors for each HI region are given in Table 2.

The values of  $f_u$  for the different momentum intervals are determined with the DeFazio-Neubert prescription, using three different forms of the shape function with the parameters,  $\Lambda^{\text{SF}}$  and  $\lambda_1^{\text{SF}}$ , determined from fits to the Belle measured photon energy spectrum in  $B \rightarrow X_s \gamma$  decays [21,22]. The resultant values of  $f_u$  are given in Table 2, they range from 3 – 32% as the lower momentum limit is decreased. The statistical uncertainty, averaged over each shape function form, is determined from the half-difference of maximum and minimum  $f_u$  found on the  $1\sigma$  error contour in  $(\Lambda^{\text{SF}}, \lambda_1^{\text{SF}})$  parameter space. The systematic error stems from variation of the scale used to evaluate strong coupling  $\alpha_s(\mu)$  ( $\mu = m_b/2, 2m_b$ ) and differences amongst shape function forms. The theoretical uncertainty is obtained by varying the parameters by  $\pm 20\%$ , reflecting the fact that the procedure is correct only to leading order in the HQET expansion that describes the non-perturbative dynamics of  $B$ -mesons. Our variation is twice that considered by CLEO ( $\pm 10\%$ ). At the time of their evaluation little was known about sub-leading and weak annihilation effects, they have since been predicted to be large [39,40,41] and are better represented by a  $\pm 20\%$  variation. The resulting full branching fractions and extracted values of  $|V_{ub}|$  are given in Table 2. All the uncertainties contributing to  $|V_{ub}|$  are summarised in Table 3 for each momentum interval. As expected, as the lower momentum cutoff is decreased, the uncertainties from  $f_u$ , in particular that due to theory, decreases, while the main experimental systematic, the estimation of  $B \rightarrow X_c e \nu_e$ , increases, in line with its background contribution. Assuming it is valid to combine experimental and theoretical uncertainties in quadrature

The best overall precision (13%) on  $|V_{ub}|$ , based on a sum in quadrature of experimental and theoretical uncertainties, is found for the  $1.9 - 2.6$  GeV/ $c$  momentum interval with

$$|V_{ub}| = (5.01 \pm 0.47 \pm 0.17 \pm 0.32 \pm 0.24) \times 10^{-3}, \quad (5)$$

where the first error is from experiment, the second and third are due to experiment and theory errors on  $f_u$ , respectively, and the last is the uncertainty in applying the  $|V_{ub}|$  extraction formula.

Table 3

Uncertainties contributing to the determination of  $|V_{ub}|(10^{-3})$  (standard method). The total error is obtained from a sum in quadrature.

Source of Uncertainty	Momentum Interval (GeV/ $c$ )					
	1.9 – 2.6	2.0 – 2.6	2.1 – 2.6	2.2 – 2.6	2.3 – 2.6	2.4 – 2.6
Statistical	0.11	0.12	0.12	0.14	0.19	0.33
$B \rightarrow X_c e \nu_e$ background	0.43	0.39	0.26	0.16	0.04	0.00
Other $B$ background	0.03	0.03	0.03	0.04	0.03	0.03
Efficiency-detector	0.12	0.11	0.11	0.10	0.11	0.12
Efficiency-model	0.04	0.04	0.05	0.05	0.05	0.08
$N_{B\overline{B}}$	0.03	0.03	0.03	0.03	0.03	0.03
$\delta_{\text{RAD}}$	0.05	0.05	0.05	0.06	0.07	0.08
$f_u$ statistical	0.17	0.19	0.22	0.26	0.35	0.51
$f_u$ systematic	0.04	0.05	0.05	0.06	0.09	0.13
$f_u$ theory	0.32	0.40	0.53	0.69	0.96	1.32
$ V_{ub}  : m_b^{\text{kin}}(1 \text{ GeV}), \lambda_{1,2}$	0.24	0.23	0.22	0.21	0.22	0.22
Total	0.64	0.66	0.69	0.81	1.07	1.48

## 5.2 BLNP method

In this prescription  $|V_{ub}|$  is obtained directly from the partial branching fraction  $\Delta B$ , using the formula

$$|V_{ub}| = \sqrt{\frac{\Delta B(1 + \delta_{\text{RAD}})}{\tau_B} \frac{1}{R}}, \quad (6)$$

where  $\tau_B$  and  $\delta_{\text{RAD}}$  are as the same as described previously, and  $R$  is the theoretical prediction of the partial rate of  $B \rightarrow X_u l \nu$  decay in units of  $|V_{ub}|^2 \text{ps}^{-1}$

Table 4

Predicted partial rate  $R$  for  $B \rightarrow X_u l \nu_l$  and extracted value of  $|V_{ub}|$  in six overlapping momentum intervals (BLNP method). The first error in  $R$  is the shape function error stemming from the uncertainty in the knowledge of HQET parameters and the second is a theoretical uncertainty stemming from the variation of the matching scales  $\mu_i, \bar{\mu}, \mu_h$ , subleading shape function models and weak annihilation effects. The first error in  $|V_{ub}|$  is the experimental error, and the remaining errors are those propagated from  $R$ , respectively.

$p_{\text{CM}} (\text{GeV}/c)$	$R ( V_{ub} ^2 \text{ps}^{-1})$	$ V_{ub}  (10^{-3})$
1.9 – 2.6	$27.74 \pm 4.00^{+2.61}_{-2.33}$	$4.49 \pm 0.42 \pm 0.32^{+0.21}_{-0.19}$
2.0 – 2.6	$21.42 \pm 3.52^{+2.13}_{-1.98}$	$4.22 \pm 0.38 \pm 0.35^{+0.21}_{-0.19}$
2.1 – 2.6	$15.29 \pm 2.89^{+1.78}_{-1.71}$	$4.07 \pm 0.28 \pm 0.38^{+0.24}_{-0.23}$
2.2 – 2.6	$9.68 \pm 2.13^{+1.62}_{-1.60}$	$3.90 \pm 0.22 \pm 0.43^{+0.33}_{-0.32}$
2.3 – 2.6	$5.12 \pm 1.33^{+1.62}_{-1.61}$	$3.97 \pm 0.21 \pm 0.52^{+0.63}_{-0.63}$
2.4 – 2.6	$2.05 \pm 0.65^{+1.54}_{-1.54}$	$4.22 \pm 0.33 \pm 0.67^{+1.58}_{-1.58}$

for a given momentum region. The implementation of the BLNP method relies on a model for the leading order shape function that is constrained by HQET parameters; the mass and average momentum squared of the  $b$ -quark, as defined in the shape function scheme, and set to  $m_b(\text{SF}) = 4.63 \text{ GeV}$  and  $\mu_\pi^2(\text{SF}) = 0.20 \text{ GeV}^2/c^2$  [18,25], respectively.

Table 4 gives the  $R$  and  $|V_{ub}|$  values for the overlapping momentum intervals. The first error on  $R$  is the experimental uncertainty on the leading order shape function, which is our own estimation calculated as the half-difference of minimum and maximum  $R$  values obtained from variations of shape function parameters suggested by BLNP authors [25]. The second error on  $R$  is a theoretical uncertainty stemming from the variation of the matching scales  $\mu_i, \bar{\mu}, \mu_h$ , sub-leading shape function models and weak annihilation effects.

Owing to larger spectral fractions predicted in this prescription, the  $|V_{ub}|$  values are systematically lower than those found by the DFN calculations detailed previously. Moreover, the shape function and theoretical errors are much improved. Our most precise value, which has an overall uncertainty of 13% as based on the sum in quadrature of all the uncertainties,

$$|V_{ub}| = (4.49 \pm 0.42 \pm 0.32^{+0.21}_{-0.19}) \times 10^{-3}, \quad (7)$$

is found for the 1.9 – 2.6 GeV/ $c$  momentum interval.

## 6 Summary

We have measured the inclusive charmless semileptonic  $B$ -meson decay branching ratio in six overlapping momentum intervals that encompass the endpoint of the electron momentum spectrum, which include a minimum lower momentum cutoff of  $1.9 \text{ GeV}/c$ . We have extracted  $|V_{ub}|$  using both the DFN and BLNP methods, but we adopt the results of the latter method since it is formulated in a consistent framework as described in the introduction. The most precise  $|V_{ub}|$  value is extracted from the decay rate in the  $1.9 - 2.6 \text{ GeV}/c$  momentum interval and found to be  $|V_{ub}| = (4.49 \pm 0.42 \pm 0.32_{-0.19}^{+0.21}) \times 10^{-3}$ . Owing to updated knowledge of background shapes and normalisations, as well as the improvement in the theoretical prediction of the decay rates for  $B \rightarrow X_u e \nu_e$  and  $B \rightarrow X_s \gamma$  decays, the precision of the present measurement is better than that of the previous endpoint measurement by CLEO [6].

## ACKNOWLEDGEMENTS

We thank the KEKB group for the excellent operation of the accelerator, the KEK cryogenics group for the efficient operation of the solenoid, and the KEK computer group and the National Institute of Informatics for valuable computing and Super-SINET network support. We acknowledge support from the Ministry of Education, Culture, Sports, Science, and Technology of Japan and the Japan Society for the Promotion of Science; the Australian Research Council, the Australian Department of Education, Science and Training, Australian Postgraduate Award and the David Hay Postgraduate Writing-Up Award; the National Science Foundation of China under contract No. 10175071; the Department of Science and Technology of India; the BK21 program of the Ministry of Education of Korea and the CHEP SRC program of the Korea Science and Engineering Foundation; the Polish State Committee for Scientific Research under contract No. 2P03B 01324; the Ministry of Science and Technology of the Russian Federation; the Ministry of Higher Education, Science and Sport of the Republic of Slovenia; the Swiss National Science Foundation; the National Science Council and the Ministry of Education of Taiwan; and the U.S. Department of Energy.

## References

- [1] K. Abe *et al.* [Belle Collaboration], Phys. Rev. Lett. **87** (2001) 091802.  
K. Abe *et al.* [Belle Collaboration], Phys. Rev. D **66** (2002) 032007.  
K. Abe *et al.* [Belle Collaboration], Phys. Rev. D **66** (2002) 071102.

- [2] B. Aubert *et al.* [BABAR Collaboration], Phys. Rev. Lett. **87** (2001) 091801.  
 B. Aubert *et al.* [BABAR Collaboration], Phys. Rev. D **66** (2002) 032003.  
 B. Aubert *et al.* [BABAR Collaboration], Phys. Rev. Lett. **89** (2002) 201802.
- [3] M. Kobayashi and T. Maskawa, Prog. Theor. Phys. **49** (1973) 652.
- [4] R. Fulton *et al.* [CLEO Collaboration], Phys. Rev. Lett. **64** (1990) 16.
- [5] J. Bartelt *et al.* [CLEO Collaboration], Phys. Rev. Lett. **71** (1993) 4111.
- [6] A. Bornheim *et al.* [CLEO Collaboration], Phys. Rev. Lett. **88** (2002) 231803.
- [7] H. Albrecht *et al.* [ARGUS Collaboration], Phys. Lett. B **234** (1990) 409.
- [8] B. Aubert *et al.* [BABAR Collaboration], Phys. Rev. Lett. **92** (2004) 071802.
- [9] H. Kakuno *et al.* [BELLE Collaboration], Phys. Rev. Lett. **92** (2004) 101801.
- [10] M. Acciarri *et al.* [L3 Collaboration], Phys. Lett. B **436** (1998) 174.
- [11] R. Barate *et al.* [ALEPH Collaboration], Eur. Phys. J. C **6** (1999) 555.
- [12] P. Abreu *et al.* [DELPHI Collaboration], Phys. Lett. B **478** (2000) 14.
- [13] G. Abbiendi *et al.* [OPAL Collaboration], Eur. Phys. J. C **21** (2001) 399.
- [14] S. W. Bosch, B. O. Lange, M. Neubert and G. Paz, Nucl. Phys. B **699** (2004) 335.
- [15] M. Neubert, Eur. Phys. J. C **40** (2005) 165.
- [16] S. W. Bosch, M. Neubert and G. Paz, JHEP **0411** (2004) 073.
- [17] M. Neubert, arXiv:hep-ph/0411027.
- [18] M. Neubert, Phys. Lett. B **612** (2005) 13.
- [19] H. F. A. Group, arXiv:hep-ex/0412073.
- [20] F. De Fazio and M. Neubert, JHEP **9906** (1999) 017.
- [21] P. Koppenburg *et al.* [Belle Collaboration], Phys. Rev. Lett. **93** (2004) 061803.
- [22] A. Limosani and T. Nozaki [Heavy Flavor Averaging Group], arXiv:hep-ex/0407052.
- [23] I. I. Y. Bigi, M. A. Shifman, N. G. Uraltsev and A. I. Vainshtein, Int. J. Mod. Phys. A **9** (1994) 2467.
- [24] M. Neubert, Phys. Rev. D **49** (1994) 4623.
- [25] B. O. Lange, M. Neubert and G. Paz, arXiv:hep-ph/0504071 and private communication with B. O. Lange, M. Neubert and G. Paz.
- [26] S. Kurokawa, Nucl. Inst rum. Meth. A **499** (2003) 1., and other papers included in this Volume.

- [27] A. Abashian *et al.* [Belle Collaboration], Nucl. Instrum. Meth. A **479** (2002) 117.
- [28] D. Scora and N. Isgur, Phys. Rev. D **52** (1995) 2783.
- [29] G. C. Fox and S. Wolfram, Phys. Rev. Lett. **41** (1978) 1581.
- [30] K. Hanagaki, H. Kakuno, H. Ikeda, T. Iijima and T. Tsukamoto, Nucl. Instrum. Meth. A **485** (2002) 490.
- [31] Events are generated with the CLEO QQ generator, see <http://www.lns.cornell.edu/public/CLEO/soft/qq>; the detector response is simulated with GEANT, R. Brun *et al.*, GEANT 3.21 CERN Report DD/EE/84-1, 1984.
- [32] S. Eidelman *et al.* [Particle Data Group], Phys. Lett. B **592** (2004) 1.
- [33] Form factors measured in J. E. Duboscq *et al.* [CLEO Collaboration], Phys. Rev. Lett. **76** (1996) 3898, are used as input to the Heavy Quark Effective Theory, see, e.g., M. Neubert, Phys. Rept. **245** (1994) 259.
- [34] R. J. Barlow and C. Beeston, Comput. Phys. Commun. **77** (1993) 219.
- [35] E. Barberio and Z. Was, Comput. Phys. Commun. **79** (1994) 291.
- [36] J. L. Goity and W. Roberts, Phys. Rev. D **51** (1995) 3459.
- [37] B. Aubert *et al.* [BABAR Collaboration], Phys. Rev. Lett. **93** (2004) 011803.
- [38] E. Richter-Was, Z. Phys. C **61** (1994) 323.
- [39] A. K. Leibovich, Z. Ligeti and M. B. Wise, Phys. Lett. B **539** (2002) 242.
- [40] C. W. Bauer, M. Luke and T. Mannel, Phys. Lett. B **543** (2002) 261.
- [41] M. Neubert, Phys. Lett. B **543** (2002) 269.